ACSNANO

www.acsnano.org

ARTICLE

Fourier-Engineered Plasmonic Lattice Resonances

Theng-Loo Lim, Yaswant Vaddi, M. Saad Bin-Alam, Lin Cheng, Rasoul Alaee, Jeremy Upham, Mikko J. Huttunen, Ksenia Dolgaleva, Orad Reshef,* and Robert W. Boyd

Cite This: https://doi.org/10.1021/acsnano.1c10710

Read Online

ACCESS | Metrics & More | Article Recommendations | Supporting Information

ABSTRACT: **Resonances in optical systems are useful for many applications, such as frequency comb generation, optical filtering, and biosensing. However, many of these applications are difficult to implement in optical metasurfaces because traditional approaches for designing multiresonant nanostructures require significant computational and fabrication efforts. To address this challenge, we introduce the concept of Fourier lattice resonances (FLRs) in which multiple desired resonances can be chosen *a priori* and used to dictate the metasurface design. Because each resonance is supported by a distinct surface lattice mode, each can have a high quality factor. Here, we experimentally demonstrate several metasurfaces with flexibly placed resonances (e.g., at 1310 and 1550 nm) and *Q*-factors as high as 800 in a plasmonic platform. This flexible procedure requires only the computation of a single Fourier transform for its design, and is based on standard lithographic fabrication methods, allowing one to design and fabricate a metasurface to fit any specific, optical-cavity-based application. This work represents a step toward the complete control over the transmission spectrum of a metasurface.**

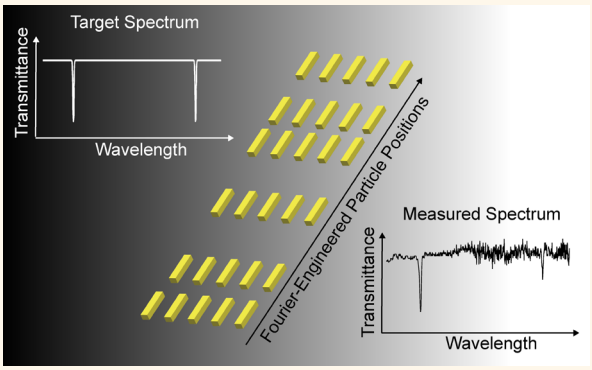

KEYWORDS: *plasmonics, metasurfaces, lattice resonances, nanoparticle arrays, nanophotonics*

Plasmonic nanoparticles are essential tools for the manipulation of light beams in metasurfaces because of the flexibility of the placement of their localized surface plasmon resonances (LSPRs).[1] The LSPR wavelength can be easily tailored since it is highly dependent on the size and the shape of the nanoparticle.[2] Additionally, LSPRs confine light in the nanoscale, leading to significant local-field enhancements.[3] Thanks to these desirable properties, many applications have been realized in a broad range of research fields such as optical filtering,[4,5] harmonic generation,[6] and biosensing.[7] However, the applications of LSPRs are limited by the intrinsic absorption loss of metals; the quality-factor of LSPRs is low (*Q*-factor <10).[8,9] One method to improve the *Q*-factor of resonant plasmonic systems is to consider instead collective optical responses of multiple nanoparticles in a periodic lattice arrangement; such metasurface-scale responses are known as surface lattice resonances (SLRs).[9−12] Unlike the LSPR, the SLR wavelength is defined by the periodicity of the positions of the nanoparticles in a periodic lattice, and this collective response has a relatively high *Q*-factor. For example, our recent work has experimentally demonstrated a *Q*-factor of 2340 around an operating wavelength of 1550 nm.[11]

In addition to improving the *Q*-factor of a lattice response, it is also highly desirable to be able to freely choose the resonance wavelengths of the metasurface.[13,14] The reason is simple: carefully tailoring multiple resonances in a metasurface allows one to customize a metasurface to specific applications, such as frequency comb generation,[15,16] ultrasensitive biosensing,[17] and fluorescence enhancements.[18] For example, methods have been proposed to tune the resonance wavelength by manipulating the dimensions of multiple particles in a single cell,[19] through plasmonic hybridization,[20] and using bound-state-in-the-continuum (BIC) modes.[21] In metasurface systems, several methods have been studied to generate and tailor multiple lattice resonances, such as utilizing multiple materials,[22] adding cladding layers to induce Fabry−Pérot SLR modes,[12] removing nanoparticles periodically,[23] using all-

Received: December 2, 2021
Accepted: March 25, 2022

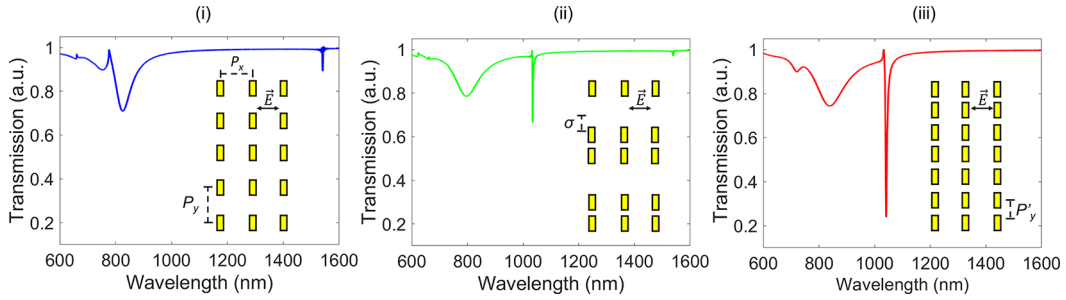

Figure 1. Bipartite Surface Lattice Resonance modes. The transmission profiles of three different lattice arrangements (i), (ii), and (iii) with their corresponding schematic drawings (see the inset figures). These lattice arrangements are made of rectangular nanoparticles, where P_y or P_y' and P_x are the lattice periodicity in the *y*-axis and *x*-axis, respectively. The incident electric field is polarized along the *x*-axis. (i) and (iii) are periodic arrays with lattice constants of P_y and P_y', respectively. For the modulated lattice arrangement (ii), every second row of particles in the array in (i) is translated by spacing $\sigma = P_y/3$. Such a system resembles the array of (iii) but with vacancies.

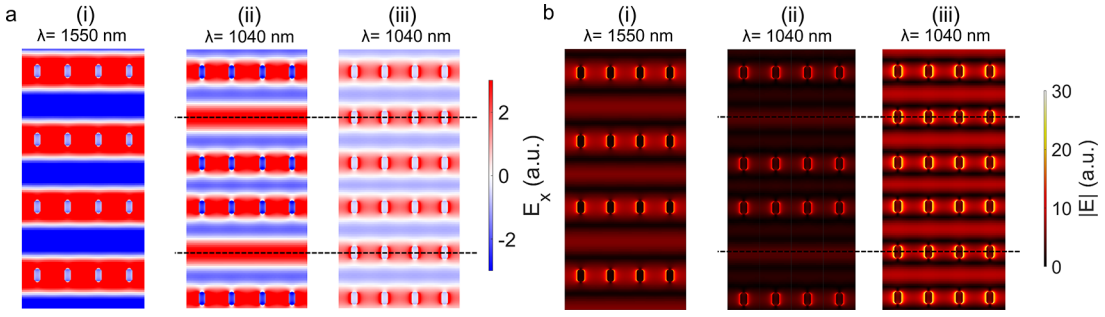

Figure 2. Near-field profiles of the lattice modes. (a) The normalized *x*-polarized electric field profiles of lattice arrangements from Figure 1, their respective SLR resonances of 1550 nm for (i) and 1040 nm for (ii) and (iii). The vacancies in every second row of the unit cell (ii) are aligned with every second row of the particles of the unit cell in (iii) (the black dashed line). The electric fields in (ii) resemble those of (iii), indicating that a similar mode is being excited. (b) The electric field amplitude profiles of the lattice arrangements, showing the field enhancement at the resonances. These results also demonstrate that all of the SLR modes possess a field enhancement within the same order of magnitude.

dielectric Mie-resonance metasurfaces,[24] and superlattice arrays.[25] Each of these methods can support multiple resonance modes; however, they are all limited in the spectral position or number of these resonances. Some methods have been developed that can define any number of resonances in flexible locations in a metasurface. In this work, we tackle this issue by exploiting a different approach: by breaking the lattice periodicity, we show that we can simultaneously introduce multiple lattice resonances with tunable resonance wavelengths. With this knowledge, we introduce and experimentally demonstrate the concept of Fourier lattice resonances (FLRs), which are a natural generalization of SLRs that can support multiple lattice resonances at desired operation wavelengths.

RESULTS AND DISCUSSION

Interpretation of Fourier Lattice Resonances (FLRs). For conceptual clarity, we begin by exploring how perturbations in translational symmetry introduce resonances. This demonstration helps interpret the physical origin of FLRs. Note that the main goal of this manuscript is *not* to reintroduce bipartite lattices,[26−29] but to motivate the theory that we will develop later on for FLRs. Consider a metasurface consisting of rectangular gold nanoparticles with a periodic lattice arrangement. The lattice is embedded in a homogeneous background of silica glass ($n \sim 1.45$), with particle dimensions of $L_x = 110$ nm and $L_y = 180$ nm and periodicities of $P_x = 500$ nm and $P_y = 1063$ nm (see the inset in Figure 1(i)). The predicted transmission spectrum for an *x*-polarized beam is calculated by the finite-difference time-domain (FDTD) method and is shown in Figure 1(i). The LSPR mode of the metasurface occurs at an operating wavelength of 830 nm, and the SLR is at 1550 nm ($\lambda_{SLR} \approx nP_y$). Next, we break the symmetry of the rectangular lattice by displacing every second row of particles by a distance $\sigma = P_y/3$ (see the inset in Figure 1(ii)). The calculated transmission profile of the metasurface is altered by this modulation (Figure 1(ii)): an additional collective resonance arises at 1040 nm. The origin of this resonance is clear when looking at Figure 1(iii), where we show a rectangular lattice of periodicity $P_y' = 2P_y/3$; the altered lattice in Figure 1(ii) resembles a sparser version of Figure 1(iii). The additional resonance is, therefore, just an SLR corresponding to the effective periodicity P_y', with an additional resonant wavelength $\lambda_{SLR}' = nP_y'$. This is further supported by examining Figure 1(iii), which shows the corresponding transmission profile with $P_y' = 2P_y/3$. Hence, the altered lattice arrangement can be viewed as combinations between two different periodic lattice arrangements. Such bipartite array lattice systems[26−29] have extensively been studied, and our numerical results are consistent with these studies.

We next examine the near-field profile of the metasurface. Figure 2a illustrates the *x*-polarized electric field of all three lattices shown in Figure 1. If we compare the electric field profile in Figure 2a (ii) with that of another perfect lattice arrangement with a periodicity of $2P_y/3$ at a wavelength of 1040 nm (Figure 2a (iii)), the same SLR modes are excited at the same wavelength. Hence, the additional SLR can be

https://doi.org/10.1021/acsnano.1c10710
ACS Nano XXXX, XXX, XXX−XXX

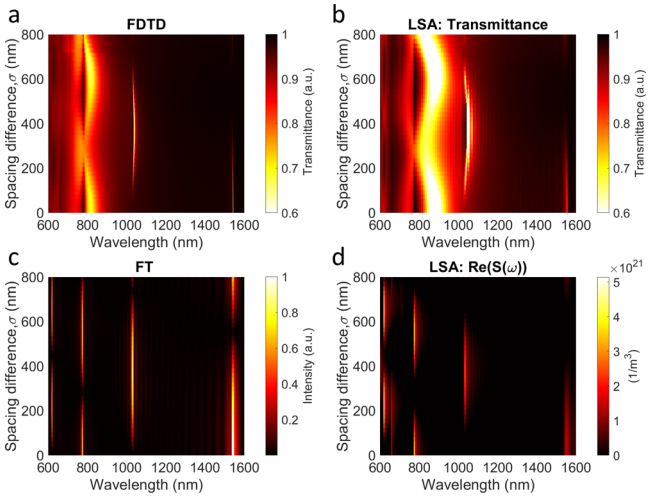

Figure 3. The evolution of the aperiodic SLR mode. (a) The FDTD-calculated transmission profiles with respects to the spacing difference σ. (b) LSA-simulated transmission spectra plotted as a function of σ. The calculated LSPR and SLR modes are largely consistent with the calculations in (a). (c) The FT-calculated power spectra with varying σ. (d) The LSA-simulated real part of lattice sum function, Re($S(\omega)$), plotted as a function of σ. The spectral features are consistent with the FT calculations in (c).

regarded as an SLR mode with a periodicity of $2P_y/3$, but missing particles.

To observe the emergence of this SLR mode, we perform a series of FDTD simulations as a function of σ. We present the simulation results in Figure 3a. As shown in this figure, for σ = 0 nm, the new SLR does not appear at 1040 nm since the lattice arrangement is still rectangular. As σ gradually increases, the periodic SLR mode at 1550 nm starts to vanish due to the cancellation produced by the particle in the unit cell being located at the antinodes of the electric field with opposite sign, and a different SLR mode begins to appear when σ is changed from 80 to 640 nm at a wavelength of 1040 nm. The most pronounced resonance occurs when $\sigma \approx 354$ nm since this corresponds to approximately a period of $2P_y/3$.

We employ the lattice sum approach (LSA)[30,31] to gain further insight into these metasurfaces. In this model, the effective polarizability induced in a single particle can be calculated by taking into account the change in the local field experienced by the particle due to the rescattered fields of the surrounding neighbor particles in the lattice. One of the main advantages of this method is that the computation time is much faster compared to a standard FDTD simulation with a superlattice element with periodic boundary conditions.[11,12] On a standard desktop computer, the LSA simulations of a 150 × 150 μm^2 lattice for the 2790 antenna placements shown in Figure 3a took ~1 min for the entire spectral sweep (600–1600 nm), whereas the FDTD simulations of two-particle superlattices with periodic boundary condition took ~1 h. Clearly, the FDTD calculation of complete metasurfaces is computationally prohibitive. In this paper, we modify the lattice sum by including the effect of σ with a lattice size of 150 × 150 μm^2, and perform the corresponding calculations concerning σ, as illustrated in Figure 3b (see also Methods). By comparing this result with that shown in Figure 3a, we demonstrate that the transmission spectra obtained by LSA calculations are in excellent agreement with FDTD simulations in terms of predicting the resonance wavelengths for the LSPR and SLR.

We are now ready to introduce the theory behind FLRs. The two SLRs in our example originate from the various periodicities present in the lattice (P_y and $2P_y/3$). Any discussions of periodicities naturally suggest the possibility of using Fourier series; indeed, we find that taking a Fourier transform (FT) of the particle locations may reveal the positions of the resonances. This idea is the essence of the design methodology of FLR metasurfaces. To demonstrate this idea by way of an example, we represent the lattice using the function $f(y)$; this function consists of a series of Gaussian profiles centered at the y-coordinates of individual nanoparticles, with a spacing corresponding to the periodicity of the actual lattice, P_y, between each profile (see Methods). We generate a series of different $f(y)$ functions for a range of values of σ (σ = 0 to 800 nm); these different $f(y)$ functions each represent a different lattice with increasing amounts of symmetry-breaking. We then take the FTs of each of these functions, and plot the resulting power spectra in Figure 3c. We compare this result to that of Figure 3d, which shows the LSA-simulated real part of lattice sum function, Re($S(\omega)$), also as a function of σ (see eq 2). The resemblance between these two figures is evident upon inspection: the power spectrum (Figure 3c) in the FT calculation has peaks in the exact wavelengths where the Re($S(\omega)$) calculation (Figure 3d) features the lattice resonances. This agreement indicates that these additional SLRs can be predicted with a simple FT of the perturbed lattices; we call this predictive design approach the Fourier lattice resonance (FLR) method. Although the SLRs for this particular lattice geometry can also be trivially explained using the Rayleigh Anomalies (RA),[32] our model introduces an additional degree of freedom in designing metasurfaces. Given that the RA model depends on periodic structures, there are many lattice arrangements which it can not treat. We can therefore view our treatment, which can consider even aperiodic lattices, as a generalization of the RA model. The additional degree of freedom will be discussed in a subsequent section.

Experimental Verifications of FLRs. To experimentally verify the FLR model, we fabricated two sets of metasurfaces consisting of rectangular nanoparticles. In Figure 4a, the images of the devices are presented; each subfigure in Figure 4a represents the actual device with different values of σ, and with a P_y of 1063 nm. This set of metasurfaces has nanoparticle dimensions of L_x = 110 nm and L_y = 180 nm, and lattice sizes of 150 × 150 μm^2. The calculated transmission spectra for these devices are shown in Figure 4b and are in good agreement with the experimental data in Figure 4c. The experimental setup and procedure are described in the Methods. As predicted, the periodic SLR mode at 1040 nm vanishes as σ decreases. Furthermore, a new SLR starts arising when σ = 88 nm, and is most prominent when σ = 354 nm, which agrees with the LSA and the FDTD simulations, supporting our theoretical interpretation. Notably, the Q-factors of this set of devices range from 80 to 90, and the sharpest aperiodic SLR dip has a Q-factor of 90 with P_y = 1063 nm and σ = 354 nm.

Our model also works with different values of P_y. Here, we fabricated another set of metasurfaces with P_y = 1598 nm (Figure 4d) and the same nanoparticle sizes as the first set of the devices. Similarly to the first set of metasurfaces, the simulated transmission profiles of the second set of

https://doi.org/10.1021/acsnano.1c10710
ACS Nano XXXX, XXX, XXX−XXX

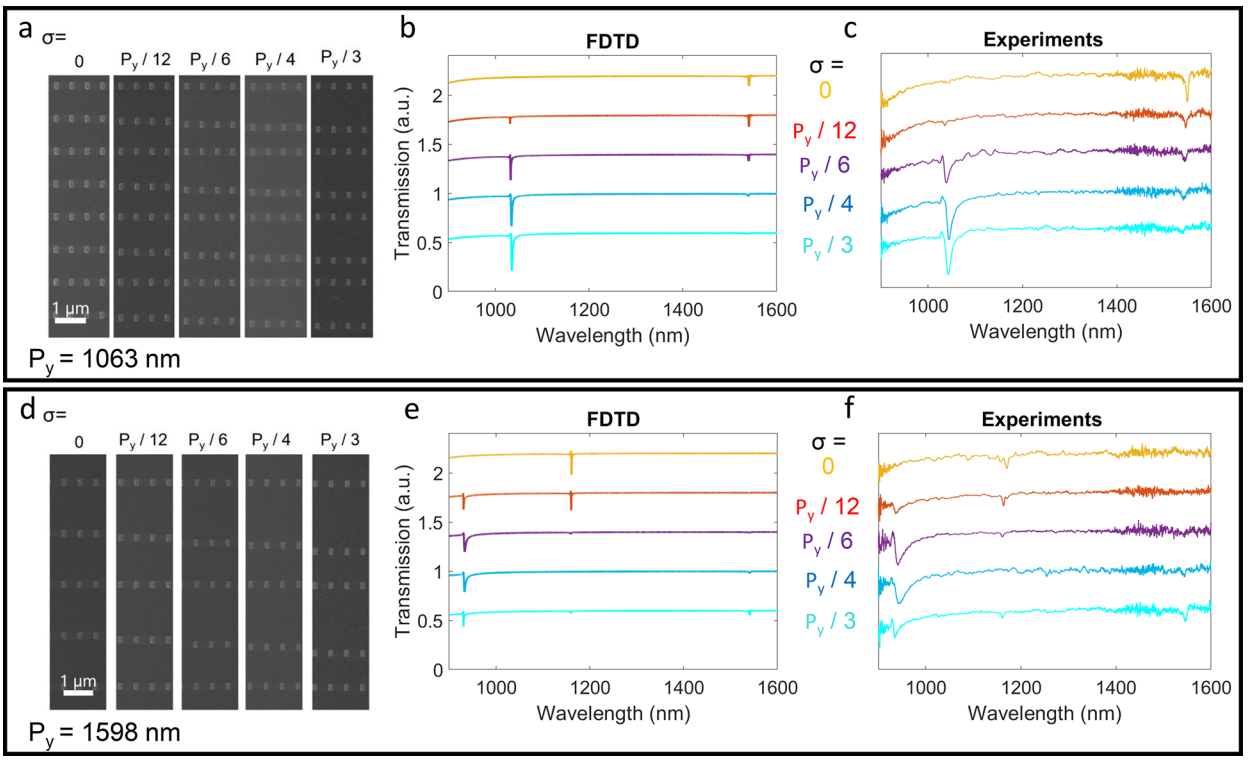

Figure 4. Experimental observation of metasurfaces with multiple SLR modes. (a,d) Helium ion microscopic images of the fabricated metasurfaces prior to cladding deposition. Each subfigure corresponds to an image with a different σ. For (a), all metasurfaces have P_y = 1063 nm, whereas for the metasurfaces in (d), P_y = 1598 nm. (b,e) The simulated transmittance of the corresponding metasurfaces with (b) P_y = 1063 nm and (e) P_y = 1598 nm. (c,f) The measured transmission spectra of the metasurfaces with (c) P_y = 1063 nm and (f) P_y = 1598 nm.

metasurfaces (P_y = 1598 nm) in Figure 4e are also in good agreement with the experimental data (Figure 4f), where a new SLR mode for this system is predicted to occur at 1550 nm and σ = 354 nm. Despite the extinction coefficients of the resonances in these metasurfaces being smaller than the first set, the *Q*-factors of these devices are relatively higher. The *Q*-factors range from 170 to 220, where the lattice resonance with the highest *Q*-factor appears at 1150 nm and σ = 532 nm. In the first set of devices, the spectral distance between the SLR at 1550 nm and the second SLR in our spectrum was 504 nm, in the second set, the distance is only 381 nm. This hints at the flexibility of modulated lattices to place SLRs at flexibly spectral locations.

We have just shown that the LSA succeeds at describing the transmission spectra of a modified lattice arrangement. However, a discrepancy arises in the *Q*-factor predicted by this method when compared to FDTD simulations and the experimental results, which we attribute to the difference in array size.[33,34] Because the nanoparticle density in the second set of metasurfaces is smaller although the array size is the same, the extinction ratio and *Q*-factor are lower than in the first set, making the second set of metasurfaces harder to characterize.

Reverse-Engineering of FLRs. Since the properties of the SLRs in bipartite lattices can be predicted by using the FLR method, in principle, the process can be reverse-engineered: one could begin with the desired transmission profile, then use the FT of that spectrum to directly engineer the nanoparticle placement to generate the desired spectrum. To demonstrate this idea, we first select a set of desired resonance wavelengths and create a virtual spectrum (Figure 5a), where we are deliberately placing two SLRs at 1150 and 1220 nm. We also include replicas of these two desired resonances represented as integer Nth harmonics in this virtual spectrum because there will naturally appear higher-order diffraction terms at $\lambda_{SLR}/2$, $\lambda_{SLR}/3$, *etc* for any lattice resonance (see Methods). Thus, the FT-simulated transmission profile of a lattice must reproduce these corresponding features. We then take the inverse FT (IFT) of the virtual spectrum (Figure 5a), which is shown in Figure 5b. Furthermore, we acquired the corresponding particle locations using a peak-finder function in Figure 5b and calculated the transmission spectra of the IFT-generated lattice arrangement using LSA with the obtained particle locations (see also Methods for more details). We observe that the corresponding SLR modes for each set are induced at the desired wavelengths (Figure 5d).

Experimental Demonstration of Reverse-Engineered FLRs. To experimentally demonstrate the reverse-engineering capabilities of the FLR method, we fabricate two devices with different sets of resonance wavelengths, one with resonances at λ = 1150 and 1220 nm (FLR1) and another, equivalent lattice prepared for resonances at λ = 1310 and 1550 nm (FLR2), where the array size is 100 × 400 μm^2 for both devices. Figure 5c shows images of subsets of the lattices for the FLR1 and FLR2 metasurfaces. After performing the measurements on these devices, we compare the LSA simulations (Figure 5d) with the experimental data (Figure 5e). The predicted resonance wavelengths from the LSA simulations are in good agreement with the experimental results of both devices. This agreement suggests that this method can be used to design resonance wavelengths flexibly. We also experimentally measured the *Q*-factors for these lattice resonances for both

https://doi.org/10.1021/acsnano.1c10710
ACS Nano XXXX, XXX, XXX−XXX

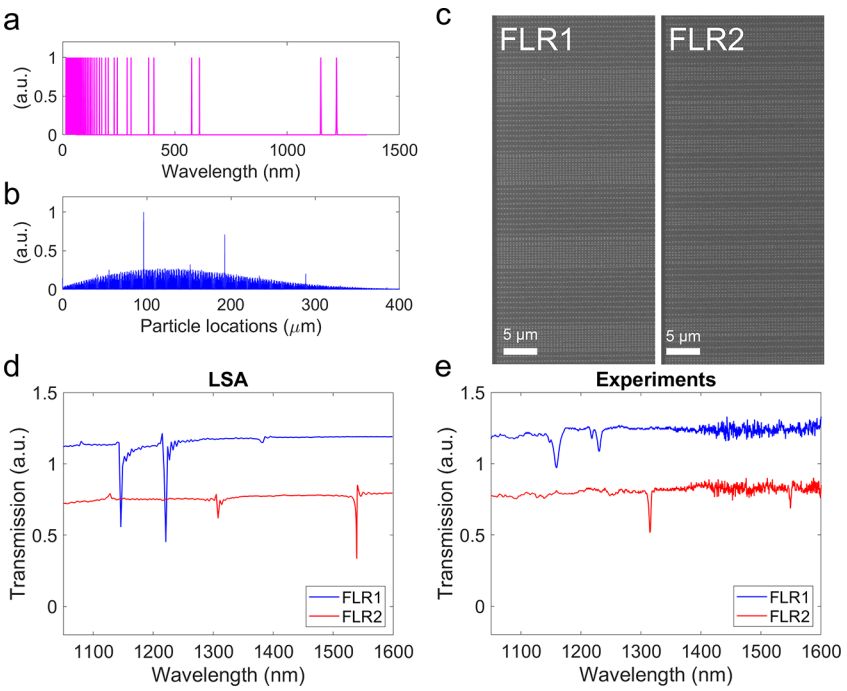

Figure 5. The FLR metasurface. (a) The generated virtual spectrum. We created a spectrum with resonance wavelengths of 1150 and 1220 nm, including their corresponding harmonics since each lattice resonance will naturally generate higher-order diffraction terms. The vertical axis of the figure is the virtual beam intensity, which we set to unity. (b) The IFT of the virtual spectrum. The *x*-axis of the diagram indicates the corresponding particle locations for the desired wavelength combination. The vertical axis of the figure is IFT power spectrum intensity; we employ a peak-finder function with a small threshold (0.015) to determine the particle locations. The superlattice for FLR1 is nonrepeating over ∼20 antenna in *y*-axis (here equivalent to ∼6 μm^2), making FDTD simulation of this device prohibitive, but still possible with LSA. (c) SEM images of subsets of the lattices for FLR1 and FLR2 metasurfaces. (d) Calculated transmission spectra of the FLR metasurfaces using LSA method. The SLRs arise at the desired wavelengths. (e) The measured transmission spectra of the corresponding FLR metasurfaces.

samples. The experimental *Q*-factors of the lattice resonances in the FLR1 metasurface are 130 at λ = 1150 nm and 200 at 1220 nm, and the experimental *Q*-factors for the FLR2 metasurface are 400 at λ = 1310 nm and 800 at 1550 nm. Fabricating the same device with a larger array size would likely increase the depth and *Q*-factor of the resonances.[11,12,34] These agreements also imply that the LSA model can be used for calculations of aperiodic lattice array.[9,11,12]

The highest *Q*-factor of these FLRs is 800 (FLR2, at a wavelength of 1550 nm), which is 2 orders of magnitude higher than those associated with the LSPRs of the individual nanoparticles and an order of magnitude higher than that of Fabry−Pérot SLR modes.[12] With such high *Q*-factors and the strong optical nonlinearity of metals,[35] the FLR metasurfaces could find applications in nonlinear processes, such as nondegenerate four-wave mixing (FWM).[36]

To consider how existing approaches could be complemented by our FLR method, we consider a few recent, key examples from the literature: a recent work showed that a single dielectric nanoparticle could be engineered to have multiple resonances, some of which showed *Q*-factors ∼190.[37] This required careful simulation of the nanoparticle dimensions and precise fabrication. By comparison, our FLR method could likely design a metasurface with similar multiple resonances from the spectrum itself. Obviously the nature of the resonators themselves are very different, but this exemplifies the ease of our design approach. Other related attempts in generating multiple resonances such as inducing Fabry−Pérot SLRs using a cladding,[12] and using orthogonal polarizations[38,39] in the lattice are often restricted to resonances that are periodic in frequency. Our method is not restricted to periodic resonances, and it only assumes dipole effects of the particles, leading to more straightforward computations.

Designing the FLR metasurface using standard FDTD simulations would be exceptionally challenging because the lack of symmetry in the lattice eliminates the possibility of simulating a small supercell, and the computational time increases with the size of the lattice arrangement.[40] In contrast, the computational time required by the FLR method is reasonable (typically within 3 min), necessitating the computation of only a single FT per lattice.

Other recent work has computed FTs to determine the 3D structure of a surface for applications in optical wavefront shaping; thus, fabricating such structure requires more sophisticated techniques.[14,41] By contrast, our work aims to find a desired transmission spectrum, and our method only utilizes standard electron-beam lithography techniques instead of 3D structures, which leads to a more straightforward fabrication.

Other related work has extensively demonstrated designing multilayer thin film stacks using FTs for applications in optical filtering.[42] Noting the similarity of our work to the study of ref.,[42] we believe that our methodology could be further extended to 3D lattices by combining our design method with the developed analytical method.

Future work on this platform could look into modifying the nanoparticle geometries to tune the width and depth of the individual resonances. Furthermore, we only took the position of the particle locations and ignored the magnitude of the

https://doi.org/10.1021/acsnano.1c10710
ACS Nano XXXX, XXX, XXX−XXX

peaks in the power spectrum when performing the IFTs. Some information is encoded in these magnitudes on the scattering amplitude of individual nanoparticles in the array. This information could perhaps be incorporated in future metasurfaces to modulate the individual extinction ratio of each resonance. Moreover, other more complex systems can be examined using our method, but are left for future studies. For example, the system could consist of arrays with complex unit cells in which the particles are placed at positions with arbitrary x- and y-coordinates, or we could consider excitation at an oblique incidence, or with the polarization not aligned to one of the array axes.

The Q-factor of the FLRs can be increased further by using dielectric particles. However, in those cases, higher-order multipoles would need to be taken into consideration.[37] In this work, we did not modify the arrangement of the particles in the x-direction. We note that such modifications should give rise to a different set of resonances that could be excited by using orthogonal polarization, that is, y-polarized light.[38] One possible application would be to modify the LSA calculations to generate orbital angular momentum (OAM) modes by introducing particle size disorders or different particle geometries.

CONCLUSIONS

We have theoretically proposed and experimentally demonstrated the concept of FLRs. The fabricated devices in this paper enable SLRs at multiple simultaneous wavelengths, and the experimental results are in good agreement with our FLR calculations. Additionally, these devices require only a standard fabrication procedure, and they can be easily expanded upon to generate multiple resonances that can be placed nearly flexibly within a spectral octave. From a broader perspective, this method is possible because we exploit a previously ignored degree of freedom by breaking the lattice periodicity, and this modeling is only possible thanks to large-scale modeling techniques like LSA. We anticipate that this design method will become significant in realizing resonant metasurfaces for many optical applications.

METHODS

Simulation. *FDTD Simulations.* A commercial three-dimensional finite-difference time-domain (FDTD) software package is utilized to perform full-wave simulations for single rectangular nanoparticles, periodic metasurfaces, and modulated metasurfaces. For the single nanoparticle simulations, the total-field scattered-field (TFSF) method is used to extract the single particle polarizability in all three dimensions: α_{xx}, α_{yy}, and α_{zz}.[43] For the periodic and modulated metasurfaces, a single unit cell was simulated using periodic boundary conditions in the in-plane dimensions and perfectly matched layers in the out-of-plane dimension. All three cases were modeled using fully dispersive optical material properties for silica and for gold.[44] Minimal artificial absorption ($\mathrm{Im}(n) \approx 10^{-4}$) was added to the background medium to reduce numerical divergences.

Lattice Sum Approach. The lattice sum approach (LSA) is a simplified version of the discrete-dipole approximation (DDA) method.[30,31] The main difference between these two methods is that the LSA assumes that the dipole moments of all interacting nanoparticles are identical. Thus, the dipole moment of any nanoparticle can be simplified as

$$\mathbf{p} = \frac{\epsilon_0 \alpha(\omega)\mathbf{E}_{\mathrm{inc}}}{1 - \epsilon_0 \alpha(\omega) S(\omega)} \equiv \epsilon_0 \alpha^*(\omega)\mathbf{E}_{\mathrm{inc}}, \tag{1}$$

where the effect of interparticle coupling is incorporated in the lattice sum $S(\omega)$, $\alpha^*(\omega)$ is the effective polarizability, and $\alpha(\omega)$ is the single nanoparticle polarizability obtained from the TFSF method. The $S(\omega)$ can be written as

$$S(\omega) = \sum_{j=1}^{N} \frac{\exp(\mathrm{i}kr_j)}{\epsilon_0 r_j}\left[k^2 + \frac{(1 - \mathrm{i}kr_j)(3\cos^2\theta_j - 1)}{r_j^2}\right] \tag{2}$$

where r_j is the spacing to the jth dipole, k is the wavenumber, and θ_j is the angle between r_j. For a periodic metasurface, r_j is just the periodicity P_v multiplied by j and the indices v indicates the x- or y-axis.

Fourier Transform of the Function f(y). The function $f(y)$ that mimics the lattice arrangement is considered by producing a series of Gaussian profiles. Each Gaussian profile represents a nanoparticle, and the Gaussian peak intensity is set to 1. We set the bandwidths of these Gaussian profiles to be significantly smaller than the spacing between the particles (bandwidth-to-spacing ratio is ∼100); thus, we can assume that the particles act like point-like dipoles under the applied incident field, similar to the assumption made in the LSA model. Next, the spacing between each Gaussian profile is P_y in the periodic case. When we considered a modulated lattice arrangement, the position of every second nanoparticle was shifted by σ. Then, we performed FT of the function with respects to y-axis, and we obtained the density plot in Figure 3c.

Combining LSA and IFT Calculations. We generate a function $f(y)$ as explained in the main text and previous subsection. This function contains a series of Gaussian peaks: two of them are placed at the desired resonance wavelengths (e.g., 1150 and 1220 nm); the remaining ones are placed at the integer harmonics for each resonance (e.g., 575 nm, 383.3 nm, 287.5 nm, ...and 610 nm, 406.7 nm, 305 nm, ..., respectively). These resonances correspond to the Rayleigh anomalies (RA) for $m = 0$:

$$\lambda \sim \frac{n}{\sqrt{\left(\frac{j}{P_y}\right)^2 + \left(\frac{m}{P_x}\right)^2}}, \tag{3}$$

where n is the refractive index, and j and m are the RA orders along the y- and x-axis, respectively. As we only consider $m = 0$ cases to simplify our model, only x-polarized beams are taken into account and P_y makes the only contribution to the system. All profiles have the same intensity, and the full width at half-maximum (fwhm) of the profiles are significantly smaller than their separation (the fwhm-to-spacing ratio is ∼100). Hence, we obtain the plot shown in Figure 5a.

We then perform an IFT of $f(y)$ (Figure 5b). The x-axis is inverted so that we are plotting against units of length instead of inverse-length. We identify the locations of the peaks in Figure 5b using a peak-finder function. The resulting list of locations correspond to the locations of the centers of the nanoparticles needed to generate the spectrum in Figure 5a.

To avoid overlap between neighboring particles, and to ensure the possibility of nanofabrication, we enforce a minimum distance between the centers of nanoparticles, here set to 250 nm. We also truncate the total number of particles at the ends of the arrays to obtain a desired array size, here 400 μm.

To determine the transmission spectra of the IFT-simulated lattice arrangement, we insert the calculated particle locations (Figure 5b) into r_j in the y-axis in eq 1. We obtain the corresponding effective $S(\omega)$ which we use to calculate α^* to determine the effective dipole moment using eq 2. We finally use α^* to obtain the transmission spectra shown in Figure 5d.

Fabrication. The metasurfaces are fabricated using a standard metal lift-off process and a positive-tone resist bilayer. We started with a fused silica substrate and defined the pattern using electron-beam lithography with the help of a commercial conductive polymer. The mask was designed using shape correction proximity error correction[45] to compensate for corner rounding. Following the development, gold was deposited using thermal evaporation. The final silica cladding layer was deposited using sputtering. The backside of

https://doi.org/10.1021/acsnano.1c10710
ACS Nano XXXX, XXX, XXX−XXX

the silica substrate was coated with an antireflective coating to minimize substrate-related etalon fringes.

Experimental Setup. A collimated broadband supercontinuum laser source was used to illuminate the devices with a wavelength spectrum ranging from 470 to 2400 nm. We used a linear polarizing optical filter to control the light beam polarization. Then, the light beam was transmitted through the device and a lens imaged the sample onto the detector array. We placed a pinhole with a diameter of 100 μm in the image plane to choose the desired metasurface. After that, the remaining light beam was guided into a multimode fiber with a diameter of 400 μm, which was coupled into an optical spectrum analyzer. Finally, we normalized the transmission spectrum of the light beam to a background trace of the substrate without gold nanostructures.

ASSOCIATED CONTENT

Supporting Information

The Supporting Information is available free of charge at https://pubs.acs.org/doi/10.1021/acsnano.1c10710.

Multiple simulated transmission profiles for a series of FLR metasurfaces with different combinations of arbitrarily selected resonance wavelengths have been demonstrated (PDF)

AUTHOR INFORMATION

Corresponding Author

Orad Reshef − *Department of Physics, University of Ottawa, Ottawa, Ontario K1N 6N5, Canada;* orcid.org/0000-0001-9818-8491; Phone: +1 (613) 562-5800 ×7138; Email: orad@reshef.ca

Authors

Theng-Loo Lim − *Department of Physics, University of Ottawa, Ottawa, Ontario K1N 6N5, Canada*

Yaswant Vaddi − *Department of Physics, University of Ottawa, Ottawa, Ontario K1N 6N5, Canada*

M. Saad Bin-Alam − *School of Electrical Engineering and Computer Science, University of Ottawa, Ottawa, Ontario K1N 6N5, Canada*

Lin Cheng − *School of Instrument and Electronics, North University of China, Taiyuan 030000, China*

Rasoul Alaee − *Department of Physics, University of Ottawa, Ottawa, Ontario K1N 6N5, Canada;* orcid.org/0000-0003-2187-4949

Jeremy Upham − *Department of Physics, University of Ottawa, Ottawa, Ontario K1N 6N5, Canada*

Mikko J. Huttunen − *Photonics Laboratory, Physics Unit, Tampere University, Tampere FI-33014, Finland;* orcid.org/0000-0002-0208-4004

Ksenia Dolgaleva − *School of Electrical Engineering and Computer Science, University of Ottawa, Ottawa, Ontario K1N 6N5, Canada*

Robert W. Boyd − *Department of Physics, University of Ottawa, Ottawa, Ontario K1N 6N5, Canada; Institute of Optics and Department of Physics and Astronomy, University of Rochester, Rochester, New York 14627, United States;* orcid.org/0000-0002-1234-2265

Complete contact information is available at: https://pubs.acs.org/10.1021/acsnano.1c10710

Author Contributions

T.L. and O.R. conceived the basic idea for this work. T.L. and Y.V. conducted the transmission measurements. T.L., O.R., and M.S.B.A. designed the experiment. R.A. and L.C. calculated single particle's polarizability. T.L. and O.R. carried out the simulations. O.R. fabricated the devices. T.L., O.R., Y.V., and J.U. analyzed the experimental results. R.W.B., J.U., M.J.H., and K.D. supervised the research and the development of the manuscript. T.L. and O.R. wrote the first draft of the manuscript, and all authors subsequently took part in the revision process and approved the final copy of the manuscript.

Notes

The authors declare no competing financial interest.

ACKNOWLEDGMENTS

We acknowledge the help of Sabaa Rashid with imaging. We thank Brian T. Sullivan and Graham Carlow for fruitful discussions. Fabrication in this work was performed in part at the Centre for Research in Photonics at the University of Ottawa (CRPuO). This research was undertaken thanks in part to funding from the Canada First Research Excellence Fund and the Canada Research Chairs program. L.C. acknowledges the support of the China Scholarship Council. M.J.H. acknowledges the Flagship of Photonics Research and Innovation (PREIN) funded by the Academy of Finland (Grant No. 320165). R.A. acknowledges support from the Alexander von Humboldt Foundation through the Feodor Lynen Return Research Fellowship. We acknowledge the support of the Natural Sciences and Engineering Research Council of Canada (NSERC) (funding reference number RGPIN/2017-06880, RGPIN/2020-03989, 950-231657, and STPGP/521619-2018). A prereview version of the manuscript has been published on the arXiv preprint server: Theng-Loo Lim; Yaswant Vaddi; M Saad Bin-Alam; Lin Cheng; Rasoul Alaee; Jeremy Upham; Mikko J Huttunen; Ksenia Dolgaleva; Orad Reshef; Robert W Boyd, *Fourier-Engineered Plasmonic Lattice Resonances*, 2021, 2112.11625, arXiv.org, https://arxiv.org/abs/2112.11625 (accessed December 22, 2021).

REFERENCES

(1) Hutter, E.; Fendler, J. H. Exploitation of localized surface plasmon resonance. *Adv. Mater.* **2004**, *16*, 1685−1706.

(2) Maier, S. A. *Plasmonics: Fundamentals and Applications*; Springer: New York, 2007.

(3) Oldenburg, S. J.; Averitt, R. D.; Westcott, S. L.; Halas, N. J. Nanoengineering of optical resonances. *Chem. Phys. Lett.* **1998**, *288*, 243−247.

(4) Yokogawa, S.; Burgos, S. P.; Atwater, H. A. Plasmonic color filters for CMOS image sensor applications. *Nano Lett.* **2012**, *12*, 4349−4354.

(5) Zeng, B.; Gao, Y.; Bartoli, F. J. Ultrathin nanostructured metals for highly transmissive plasmonic subtractive color filters. *Sci. Rep.* **2013**, *3*, 2840.

(6) Palomba, S.; Danckwerts, M.; Novotny, L. Nonlinear plasmonics with gold nanoparticle antennas. *J. Opt. A: Pure Appl. Opt.* **2009**, *11*.114030

(7) Qiu, G.; Gai, Z.; Saleh, L.; Tang, J.; Gui, T.; Kullak-Ublick, G. A.; Wang, J. Thermoplasmonic-Assisted Cyclic Cleavage Amplification for Self-Validating Plasmonic Detection of SARS-CoV-2. *ACS Nano* **2021**, *15*, 7536−7546.

(8) Doiron, B.; Mota, M.; Wells, M. P.; Bower, R.; Mihai, A.; Li, Y.; Cohen, L. F.; Alford, N. M. N.; Petrov, P. K.; Oulton, R. F.; Maier, S. A. Quantifying Figures of Merit for Localized Surface Plasmon Resonance Applications: A Materials Survey. *ACS Photonics* **2019**, *6*, 240−259.

(9) Kravets, V. G.; Kabashin, A. V.; Barnes, W. L.; Grigorenko, A. N. Plasmonic Surface Lattice Resonances: A Review of Properties and Applications. *Chem. Rev.* **2018**, *118*, 5912−5951.

(10) Utyushev, A. D.; Zakomirnyi, V. I.; Rasskazov, I. L. Collective lattice resonances: Plasmonics and beyond. *Reviews in Physics* **2021**, *6*, 100051.
(11) Bin-Alam, M. S.; Reshef, O.; Mamchur, Y.; Alam, M. Z.; Carlow, G.; Upham, J.; Sullivan, B. T.; Ménard, J.-M.; Huttunen, M. J.; Boyd, R. W. Ultra-high-Q resonances in plasmonic metasurface. *Nat. Commun.* **2021**, *12*, 974.
(12) Reshef, O.; Saad-Bin-Alam, M.; Huttunen, M. J.; Carlow, G.; Sullivan, B. T.; Ménard, J. M.; Dolgaleva, K.; Boyd, R. W. Multiresonant High- Q Plasmonic Metasurfaces. *Nano Lett.* **2019**, *19*, 6429−6434.
(13) Molesky, S.; Lin, Z.; Piggott, A. Y.; Jin, W.; Vucković, J.; Rodriguez, A. W. Inverse design in nanophotonics. *Nat. Photonics* **2018**, *12*, 659−670.
(14) Lassaline, N.; Brechbühler, R.; Vonk, S. J.; Ridderbeek, K.; Spieser, M.; Bisig, S.; le Feber, B.; Rabouw, F. T.; Norris, D. J. Optical Fourier surfaces. *Nature* **2020**, *582*, 506−510.
(15) Okawachi, Y.; Saha, K.; Levy, J. S.; Wen, Y. H.; Lipson, M.; Gaeta, A. L. Octave-spanning frequency comb generation in a silicon nitride chip. *Opt. Lett.* **2011**, *36*, 3398.
(16) Kippenberg, T. J.; Holzwarth, R.; Diddams, S. A. Microresonator-based optical frequency combs. *Science* **2011**, *332*, 555−559.
(17) Menezes, J. W.; Ferreira, J.; Santos, M. J.; Cescato, L.; Brolo, A. G. Large-area fabrication of periodic arrays of nanoholes in metal films and their application in biosensing and plasmonic-enhanced photovoltaics. *Adv. Funct. Mater.* **2010**, *20*, 3918−3924.
(18) Vecchi, G.; Giannini, V.; Gómez Rivas, J. Shaping the fluorescent emission by lattice resonances in plasmonic crystals of nanoantennas. *Phys. Rev. Lett.* **2009**, *102*, 2−5.
(19) Fradkin, I. M.; Dyakov, S. A.; Gippius, N. A. Nanoparticle lattices with bases: Fourier modal method and dipole approximation. *Phys. Rev. B* **2020**, *102*, 045432.
(20) Baur, S.; Sanders, S.; Manjavacas, A. Hybridization of Lattice Resonances. *ACS Nano* **2018**, *12*, 1618−1629.
(21) Abujetas, D. R.; Olmos-Trigo, J.; Sáenz, J. J.; Sánchez-Gil, J. A. Coupled electric and magnetic dipole formulation for planar arrays of particles: Resonances and bound states in the continuum for all-dielectric metasurfaces. *Phys. Rev. B* **2020**, *102*, 125411.
(22) Hsu, C. W.; Zhen, B.; Qiu, W.; Shapira, O.; DeLacy, B. G.; Joannopoulos, J. D.; Soljačić, M. Transparent displays enabled by resonant nanoparticle scattering. *Nat. Commun.* **2014**, *5*, 3152.
(23) Zundel, L.; May, A.; Manjavacas, A. Lattice Resonances Induced by Periodic Vacancies in Arrays of Nanoparticles. *ACS Photonics* **2021**, *8*, 360−368.
(24) Kuznetsov, A. I.; Miroshnichenko, A. E.; Brongersma, M. L.; Kivshar, Y. S.; Luk'yanchuk, B. Optically resonant dielectric nanostructures. *Science* **2016**, *354*. DOI: 10.1126/science.aag2472
(25) Wang, D.; Yang, A.; Hryn, A. J.; Schatz, G. C.; Odom, T. W. Superlattice Plasmons in Hierarchical Au Nanoparticle Arrays. *ACS Photonics* **2015**, *2*, 1789−1794.
(26) Kravets, V.; Schedin, F.; Grigorenko, A. Extremely narrow plasmon resonances based on diffraction coupling of localized plasmons in arrays of metallic nanoparticles. *Physical review letters* **2008**, *101*, 087403.
(27) Humphrey, A.; Barnes, W. Plasmonic surface lattice resonances in arrays of metallic nanoparticle dimers. *Journal of Optics* **2016**, *18*, 035005.
(28) Mahi, N.; Leveque, G.; Saison, O.; Marae-Djouda, J.; Caputo, R.; Gontier, A.; Maurer, T.; Adam, P.-M.; Bouhafs, B.; Akjouj, A. In depth investigation of lattice plasmon modes in substrate-supported gratings of metal monomers and dimers. *J. Phys. Chem. C* **2017**, *121*, 2388−2401.
(29) Cuartero-González, A.; Sanders, S.; Zundel, L.; Fernández-Domínguez, A. I.; Manjavacas, A. Super-and subradiant lattice resonances in bipartite nanoparticle arrays. *ACS Nano* **2020**, *14*, 11876−11887.
(30) Draine, B. T.; Flatau, P. J. Discrete-Dipole Approximation For Scattering Calculations. *Journal of the Optical Society of America A* **1994**, *11*, 1491.
(31) Zou, S.; Janel, N.; Schatz, G. C. Silver nanoparticle array structures that produce remarkably narrow plasmon lineshapes. *J. Chem. Phys.* **2004**, *120*, 10871−10875.
(32) Rayleigh, L. On the dynamical theory of gratings. *Proceedings of the Royal Society of London. Series A, Containing Papers of a Mathematical and Physical Character* **1907**, *79*, 399−416.
(33) Rodriguez, S. R.; Schaafsma, M. C.; Berrier, A.; Gómez Rivas, J. Collective resonances in plasmonic crystals: Size matters. *Physica B: Condensed Matter* **2012**, *407*, 4081−4085.
(34) Zundel, L.; Manjavacas, A. Finite-size effects on periodic arrays of nanostructures. *JPhys. Photonics* **2019**, *1*.015004
(35) Bin-Alam, M. S.; Baxter, J.; Awan, K. M.; Kiviniemi, A.; Mamchur, Y.; Lesina, A. C.; Tsakmakidis, K. L.; Huttunen, M. J.; Ramunno, L.; Dolgaleva, K. Hyperpolarizability of plasmonic meta-atoms in metasurfaces. *Nano Lett.* **2021**, *21*, 51−59.
(36) Boyd, R. W. *Nonlinear Opt.*; Academic Press: Cambridge, 2020.
(37) Koshelev, K.; Kruk, S.; Melik-Gaykazyan, E.; Choi, J. H.; Bogdanov, A.; Park, H. G.; Kivshar, Y. Subwavelength dielectric resonators for nonlinear nanophotonics. *Science* **2020**, *367*, 288−292.
(38) Huttunen, M. J.; Reshef, O.; Stolt, T.; Dolgaleva, K.; Boyd, R. W.; Kauranen, M. Efficient nonlinear metasurfaces by using multiresonant high-Q plasmonic arrays. *Journal of the Optical Society of America B* **2019**, *36*, No. E30.
(39) Bin-Alam, M. S.; Reshef, O.; Ahmad, R. N.; Upham, J.; Huttunen, M. J.; Dolgaleva, K.; Boyd, R. W. *Cross-polarized surface lattice resonances in a rectangular lattice plasmonic metasurface*. 2021, *2111*.02472, arXiv.org, DOI: 10.48550/arXiv.2111.02472 (accessed 2021/11/3).
(40) Lesina, A. C.; Vaccari, A.; Berini, P.; Ramunno, L. *FDTD method and HPC for large-scale computational nanophotonics*; Springer: Dordrecht, 2017.
(41) Mamin, H. J.; Rugar, D. Thermomechanical writing with an atomic force microscope tip. *Appl. Phys. Lett.* **1992**, *61*, 1003−1005.
(42) Dobrowolski, J. A.; Lowe, D. Optical thin film synthesis program based on the use of Fourier transforms. *Appl. Opt.* **1978**, *17*, 3039.
(43) Alaee, R.; Albooyeh, M.; Rockstuhl, C. Theory of metasurface based perfect absorbers. *J. Phys. D: Appl. Phys.* **2017**, *50*.503002
(44) Johnson, P. B.; Christy, R. W. Optical Constant of the Nobel Metals. *Phys. Rev. B* **1972**, *6*, 4370−4379.
(45) Schulz, S. A.; Upham, J.; Bouchard, F.; De Leon, I.; Karimi, E.; Boyd, R. W. Quantifying the impact of proximity error correction on plasmonic metasurfaces [Invited]. *Optical Materials Express* **2015**, *5*, 2798.

https://doi.org/10.1021/acsnano.1c10710
ACS Nano XXXX, XXX, XXX−XXX